

Covariant Helmholtz-Hodge Decomposition: Resolving Spurious Vorticity via Acoustic Geometry

Chanho Park,¹ Yeachan Kwak,¹ and Seongim Choi¹

¹*School of Mechanical Engineering, Gwangju Institute of Science and Technology, Gwangju 61005, Republic of Korea*

The separation of acoustic and vortical fluctuations in compressible turbulence becomes ambiguous in thermodynamically inhomogeneous media, where refraction by entropy gradients and shocks can be misclassified as solenoidal content by Euclidean post-processing. We introduce a covariant Helmholtz–Hodge decomposition (CHHD) with respect to an effective acoustic metric, which identifies the irrotational (potential) component with the exact part of the metric-dual velocity one-form. Thermal refraction and shock-induced bending are absorbed into the induced curvature, ensuring that such geometric variations are not misidentified as physical vorticity. For canonical entropy-spot refraction and normal-shock discontinuities, Euclidean Helmholtz–Hodge and momentum-potential post-processing produce significant leakage in the refracting/discontinuous region, whereas the covariant splitting remains at the numerical noise floor (typically $\lesssim 10^{-12}$) throughout the domain, demonstrating robustness even at the sonic horizon, where the Euclidean metric singularity typically causes catastrophic error amplification. This geometric framework for velocity fields resolves the ambiguity of irrotational motion in inhomogeneous media and establishes a necessary foundation for future generalizations to full thermodynamic state vectors.

Introduction— Separating radiating (acoustic) fluctuations from non-radiating (hydrodynamic) motions in compressible turbulence is essential for source identification, reduced-order modeling, and interpreting high-fidelity simulations in Computational Aeroacoustics (CAA) [1–4]. Since Lighthill’s analogy and its extensions [5–8], CAA has developed mean-flow-aware wave operators and numerical methods that decouple generation and propagation [9–13]. In snapshot-based LES/DNS post-processing, the same goal is pursued via instantaneous splittings, including velocity-based Helmholtz–Hodge decompositions (HHD) [14–18] and Doak’s Momentum Potential Theory (MPT) applied to momentum density [19–21], alongside complementary vortex-sound, modal, and perturbation-equation approaches [22–31].

The fundamental barrier, however, is not numerical precision, but geometric consistency. Standard HHD uses Euclidean inner products and Euclidean curl, implicitly assuming flat background geometry. In thermodynamically non-uniform or strongly accelerated media, acoustic propagation is refracted by sound-speed gradients and non-uniform mean flow [32–34]. When represented in a flat Euclidean frame, a refracted (bent) acoustic field can exhibit an apparent nonzero Euclidean curl and is misclassified as solenoidal content—often reported as spurious vorticity or spectral leakage [16, 17]. The ambiguity is exacerbated near shocks and in shock–turbulence interaction [35–37], and momentum-based splittings can retain substantial solenoidal content in $\rho\mathbf{u}$ even when the underlying velocity field is refraction-dominated rather than vortical [21]. While analogous geometric frameworks exist in cosmological perturbation theory [38] and transformation optics [39], practical separations in anisotropic seismology often rely on non-local Fourier filtering or pseudo-Helmholtz approximations that lack exact spatial locality [40]. Furthermore, these formulations

typically address static material anisotropy (spatial curvature) rather than the convective symmetry breaking (spacetime curvature) inherent to a moving compressible fluid.

In this Letter, we address this ambiguity by aligning the decomposition geometry with acoustic propagation physics. Building on Gordon’s optical metric [41] and analogue-gravity formulations of sound [42–46], we treat the non-uniform background as an effective Lorentzian spacetime for acoustic perturbations. On each time slice, this induces a spatial Riemannian metric that defines the natural inner product for splitting. We leverage this geometric framework to generalize the Helmholtz–Hodge (Hodge) splitting with respect to this acoustically privileged metric: the irrotational (potential) component is identified with the exact part of the metric-dual velocity one-form, while vortical content is diagnosed intrinsically via $d(u^b)$ and its Hodge dual, preventing refraction from masquerading as vorticity under Euclidean post-processing. We validate the approach on canonical entropy-spot and normal-shock configurations, where Euclidean HHD and MPT exhibit significant leakage, while the metric-aligned splitting maintains separation at the numerical noise floor throughout the domain, effectively handling the metric-degenerate (sonic-horizon) set via consistent regularization. This yields a robust route to mode isolation in extreme thermo-fluid environments relevant to high-speed propulsion and reacting flows [11, 25].

Covariant Helmholtz–Hodge Decomposition in Acoustic Geometry— Let $\Omega \subset \mathbb{R}^3$ be the spatial domain. We consider a stationary, inhomogeneous background state defined by density ρ_0 , pressure p_0 , velocity \mathbf{U}_0 , and sound speed c_0 , obtained in practice from a mean flow, low-pass filter, or Reynolds average. The instantaneous velocity field is decomposed into this background and a fluctuation, $\mathbf{u}(\mathbf{x}, t) = \mathbf{U}_0(\mathbf{x}) + \mathbf{u}'(\mathbf{x}, t)$. Our objective is to

split \mathbf{u}' into an irrotational (potential) component and a complementary vortical component in a manner consistent with the effective geometry of sound propagation. Here we focus on a velocity-field decomposition; in general compressible flows, a distinct entropy contribution is not identifiable from velocity snapshots alone and requires augmenting the state space to the full thermodynamic perturbation vector. For the canonical configurations considered here, entropy fluctuations act primarily through slow modulation of the background fields (notably $c_0(\mathbf{x})$ and $\rho_0(\mathbf{x})$), so their leading-order aeroacoustic effect is refraction, which is already encoded in the effective acoustic geometry induced by the background flow.

Linear acoustic perturbations on a moving inhomogeneous background can be written in a covariant form using an effective Lorentzian metric (Gordon/analogue-gravity formulation) [41–44].,

$$\square_g \psi \equiv \frac{1}{\sqrt{-g}} \partial_\mu (\sqrt{-g} g^{\mu\nu} \partial_\nu \psi) = 0, \quad (1)$$

where ψ is an acoustic potential variable and $g_{\mu\nu}$ encodes $(\rho_0, \mathbf{U}_0, c_0)$. On each time slice, the principal spatial part of the inverse metric defines an acoustically privileged spatial metric tensor. In Euclidean Cartesian coordinates, we use

$$\gamma^{ij} \equiv \delta^{ij} - \frac{U_0^i U_0^j}{c_0^2}, \quad (2)$$

with inverse

$$\gamma_{ij} = \delta_{ij} + \frac{U_{0i} U_{0j}}{c_0^2 - |\mathbf{U}_0|^2}, \quad \gamma \equiv \det(\gamma_{ij}). \quad (3)$$

The tensor γ_{ij} defines the acoustically privileged geometry used in the projection. Spatial variability in $c_0(\mathbf{x})$ and $\mathbf{U}_0(\mathbf{x})$ enters only through the spatial dependence of γ_{ij} . In the Euclidean limit ($\mathbf{U}_0 = \mathbf{0}$), the classical Helmholtz decomposition is recovered, so the present approach provides a natural acoustic generalization of irrotational content.

Given the fluctuation velocity \mathbf{u}' (a contravariant vector field), define its metric-dual 1-form via the musical isomorphism,

$$\mathbf{u}^b \equiv u_i dx^i, \quad u_i \equiv \gamma_{ij} u'^j. \quad (4)$$

The irrotational (potential) component (denoted hereafter as \mathbf{u}_{ac}) is defined as the exact part of this 1-form:

$$\mathbf{u}_{ac}^b = d\phi, \quad \Rightarrow \quad u_{ac}^i = (\nabla_\gamma \phi)^i \equiv \gamma^{ij} \partial_j \phi, \quad (5)$$

so that lowering the index recovers a pure gradient 1-form, $u_{ac,i} = \gamma_{ij} u_{ac}^j = \partial_i \phi$. This is the precise sense in which sound remains irrotational: it is irrotational with respect to the geometry that governs its propagation.

Why Euclidean Helmholtz–Hodge splitting leaks in non-uniform media— The root cause of spurious vorticity in standard post-processing is not that sound ceases to be potential, but that the notion of irrotational velocity implicitly depends on how one identifies a velocity vector with a covector (1-form). In Euclidean HHD, this identification is performed with δ_{ij} : $\mathbf{u}_E^b = (\delta_{ij} u'^j) dx^i$, and irrotationality is tested through the Euclidean curl of the vector field (equivalently through $d(\mathbf{u}_E^b)$). In an inhomogeneous moving medium, however, the acoustically natural identification is metric-dependent, $\mathbf{u}^b = (\gamma_{ij} u'^j) dx^i$; the potential component is exact in this geometry, $\mathbf{u}_{ac}^b = d\phi$, so $d(\mathbf{u}_{ac}^b) \equiv 0$ independent of ∇c_0 and $\nabla \mathbf{U}_0$.

The mismatch becomes explicit when one expresses a covariantly potential acoustic field in Euclidean operators. If $\mathbf{u}_{ac}^b = d\phi$, then the associated contravariant components are $u_{ac}^i = \gamma^{ij} \partial_j \phi$, which is generally not a Euclidean gradient field. Consequently, the Euclidean curl does not vanish and produces an apparent solenoidal content [16]:

$$\begin{aligned} (\nabla \times \mathbf{u}_{ac})_E^k &= \epsilon^{kij} \partial_i u_{ac}^j = \epsilon^{kij} \partial_i (\gamma^{jm} \partial_m \phi) \\ &= \epsilon^{kij} (\partial_i \gamma^{jm}) \partial_m \phi + \epsilon^{kij} \gamma^{jm} \partial_i \partial_m \phi. \end{aligned} \quad (6)$$

where ϵ^{kij} is the Levi-Civita permutation symbol. Both terms vanish in the uniform-medium limit ($\gamma^{ij} = \delta^{ij}$), recovering the classical identity $\nabla \times \nabla \phi \equiv 0$. In non-uniform backgrounds, the coefficient-gradient contribution $\partial_i \gamma^{jm}$ is generically nonzero and scales with ∇c_0 and $\nabla \mathbf{U}_0$; it represents refraction/anisotropy encoded by the medium, not the creation of physical vortical motion. This is precisely why Euclidean HHD can label thermally refracted sound (entropy spots) or shock-induced bending as vorticity, whereas the intrinsic diagnostic introduced below recognizes $\mathbf{u}_{ac}^b = d\phi$ as curl-free in the acoustically privileged geometry.

Computing ϕ (projection via a Laplace–Beltrami solve)— To obtain ϕ from data, we project \mathbf{u}^b onto the space of exact 1-forms under the γ -inner product. Applying the codifferential δ_γ to (5) yields the Laplace–Beltrami problem

$$\Delta_\gamma \phi \equiv \frac{1}{\sqrt{\gamma}} \partial_i (\sqrt{\gamma} \gamma^{ij} \partial_j \phi) = \nabla_\gamma \cdot \mathbf{u}' \equiv \frac{1}{\sqrt{\gamma}} \partial_i (\sqrt{\gamma} u'^i), \quad (7)$$

with boundary conditions chosen to enforce a well-posed splitting. For a bounded domain, the natural analogue of the standard Neumann condition is

$$(\nabla_\gamma \phi)^i n_i = u'^i n_i \quad \text{on } \partial\Omega, \quad (8)$$

which ensures the complementary component has no normal flux, $u_{\text{vort}}^i n_i = 0$. (For periodic domains, ϕ is computed up to an arbitrary constant, fixed by setting $\langle \phi \rangle_\Omega = 0$.)

While the standard Neumann closure Eq. (8) is deliberately employed in this Letter to isolate the geometric

resolution of interior refraction from boundary effects, strictly enforcing zero vortical flux can be restrictive for general open-boundary flows. To address this limitation in future applications, we provide a rigorous generalization of the Natural HHD [15] to the present geometric framework. By minimizing the kinetic energy functional $E[\phi, \Psi] = \frac{1}{2} \int_{\Omega} \|\mathbf{u}^p - d\phi - \delta\Psi\|_{\gamma}^2 dV_{\gamma}$ with respect to both scalar (ϕ) and vector (Ψ) potentials, the decomposition reduces to a monolithic linear system that determines both components simultaneously. Crucially, unlike iterative boundary correction methods, this covariant formulation structurally enforces orthogonality via the acoustic metric γ_{ij} , allowing the optimal flux partitioning to be resolved in a single step (see End Matter for the mathematical derivation). Although not implemented for the present canonical benchmarks, this one-shot variational framework provides a clear mathematical pathway for handling arbitrary open boundaries.

Having solved (7)–(8), we define

$$u_{\text{vort}}^i \equiv u'^i - u_{\text{ac}}^i. \quad (9)$$

Intrinsic (metric-consistent) vorticity diagnostic— To quantify leakage and to avoid Euclidean misclassification under refraction, we measure vorticity intrinsically as

$$\zeta_{\text{cov}} \equiv \star_{\gamma} d(\mathbf{u}^b), \quad (10)$$

where d is the exterior derivative and \star_{γ} is the Hodge star induced by γ . In components, for a 3D slice,

$$\begin{aligned} \zeta_{\text{cov}}^k &= \frac{1}{2\sqrt{\gamma}} \epsilon^{kij} (\partial_i u_j - \partial_j u_i) \\ &= \frac{1}{2\sqrt{\gamma}} \epsilon^{kij} [\partial_i (\gamma_{jm} u'^m) - \partial_j (\gamma_{im} u'^m)]. \end{aligned} \quad (11)$$

For the acoustically defined component $\mathbf{u}_{\text{ac}}^b = d\phi$, one obtains $d(d\phi) = 0$ identically, hence

$$\zeta_{\text{cov}}(\mathbf{u}_{\text{ac}}) \equiv \mathbf{0}. \quad (12)$$

Transonic regions and shock discontinuities— The spatial metric becomes ill-conditioned as $|\mathbf{U}_0|/c_0 \rightarrow 1$. Specifically, when $|\mathbf{U}_0| < c_0$, γ_{ij} is symmetric positive definite and furnishes a Riemannian inner product, yielding an elliptic Laplace–Beltrami operator. In transonic and supersonic regions ($|\mathbf{U}_0| \geq c_0$), however, the metric becomes degenerate or indefinite, corresponding to a sonic horizon in the analogue-spacetime interpretation. This streamwise metric divergence is illustrated in Fig. 1, which also shows that entropy injection (higher c_0) shifts the singularity to higher velocities, providing a partial stabilizing effect on the geometry. Despite this shift, the mathematical singularity necessitates explicit numerical treatment. To address this, we apply a horizon regularization by replacing the denominator $c_0^2 - |\mathbf{U}_0|^2$ with $\max(c_0^2 - |\mathbf{U}_0|^2, \epsilon_{\text{reg}}^2)$. This regularization ensures that

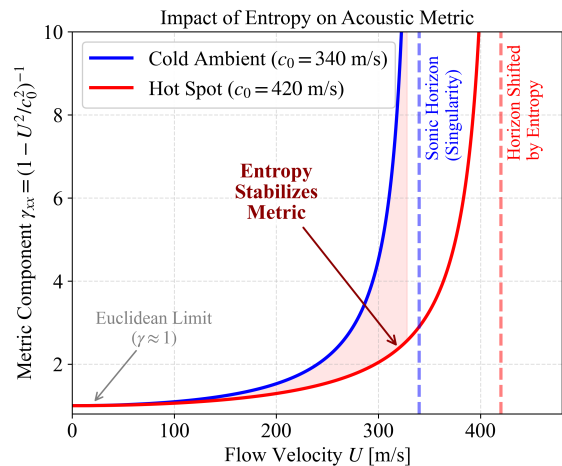


FIG. 1: Thermodynamic stabilization of the acoustic metric. The streamwise metric component γ_{xx} diverges at the sonic horizon ($U = c_0$). Crucially, entropy injection (higher c_0) shifts this horizon, effectively stabilizing the metric in the region of interest.

the effective metric remains positive definite, maintaining a well-posed (coercive) elliptic projection even in supersonic zones. Since the Helmholtz decomposition is inherently a global elliptic characterization of the instantaneous state (distinct from hyperbolic wave propagation), this regularization effectively defines the supersonic potential component as the continuous limit of the subsonic solution, preserving the topological continuity of the decomposition.

Crucially, to strictly enforce the inverse property $\gamma^{ik}\gamma_{kj} = \delta_j^i$ even under regularization, we compute the contravariant metric γ^{ij} as the numerical matrix inverse of the regularized covariant metric γ_{ij} , rather than evaluating Eq. (2) independently. Furthermore, spatial derivative operators are constructed as Kronecker products of one-dimensional difference matrices (e.g., $\mathbf{D}_x = \mathbf{I}_y \otimes \mathbf{D}_x^{1D}$). This guarantees the discrete commutativity of cross-derivatives ($\mathbf{D}_x \mathbf{D}_y = \mathbf{D}_y \mathbf{D}_x$) on bounded domains. Using these consistent operators ensures that the geometric identity $\zeta_{\text{cov}}(\mathbf{u}_{\text{ac}}) \equiv \mathbf{0}$ holds to the numerical noise floor, regardless of metric gradients or topology.

Numerical Validation— Equation (7) is discretized in conservative form and solved using the same discrete derivative operators for both projection and diagnostics to ensure that $\zeta_{\text{cov}}(\mathbf{u}_{\text{ac}}) \equiv \mathbf{0}$ holds to the numerical noise floor. We test the splitting on two benchmarks that violate Euclidean assumptions: an entropy spot (strong ∇c_0 refraction) and a stationary normal shock ($M = 1.5 \rightarrow 0.7$). Detailed definitions of the background flow profiles, acoustic perturbations, grid resolutions, and boundary treatments are provided in the End Matter. In each case, we prescribe a purely acoustic perturbation via a potential ϕ and assess whether refraction or

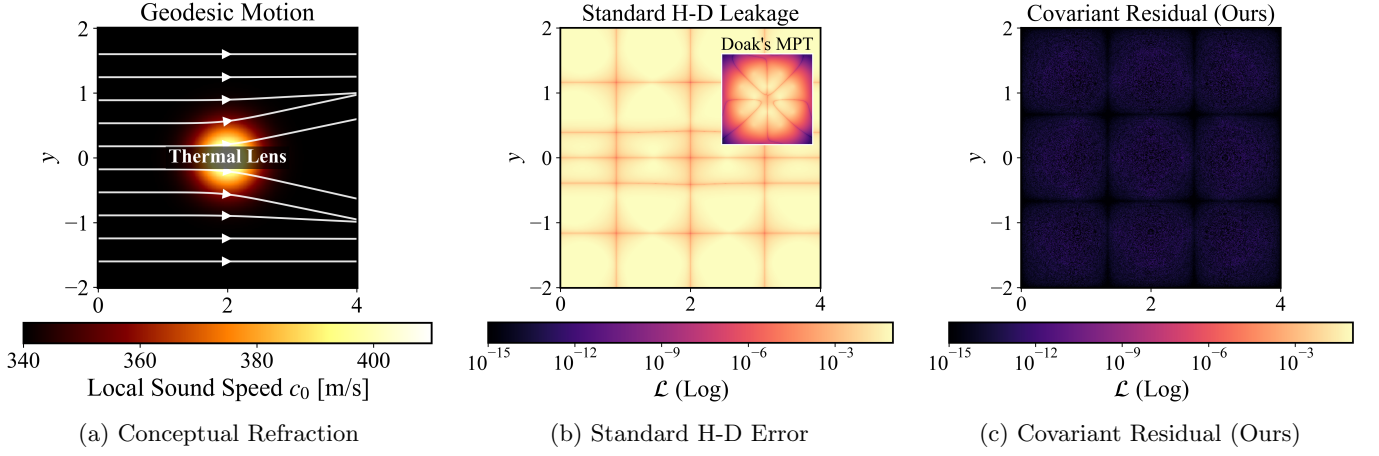


FIG. 2: Visualizing separation in a thermal entropy spot. (a) Conceptual ray tracing showing geodesic bending of acoustic paths due to ∇c_0 . (b) Euclidean HHD misinterprets this refraction as spurious vorticity $|\boldsymbol{\omega}|$ (bright structures). Inset: Doak’s MPT diagnostic. (c) The covariant residual ζ_{cov} remains at the numerical floor, consistent with geometric absorption of thermal refraction.

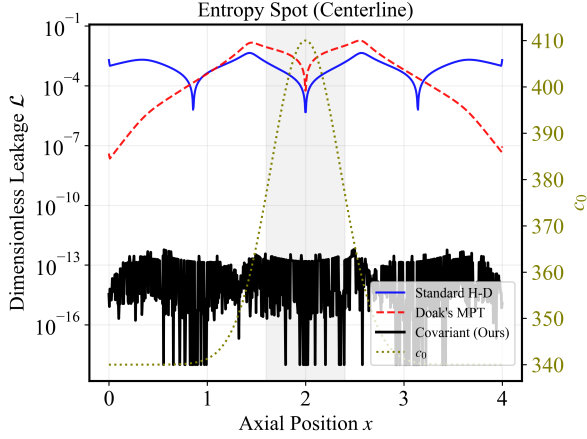


FIG. 3: Entropy-spot validation (centerline leakage). Centerline $\mathcal{L}(x, y = 0)$ defined by Eq. (13). Euclidean HHD exhibits high-amplitude leakage across the entire wave packet, and Doak’s MPT exhibits pronounced, spatially distributed artifacts inside the thermal lens despite improved far-field behavior, whereas the covariant splitting remains at the numerical noise floor ($\mathcal{L} \lesssim 10^{-12}$) throughout the domain.

discontinuities are spuriously classified as solenoidal content. We compare the present metric-aligned splitting with Euclidean Helmholtz–Hodge decomposition (HHD) and Doak’s momentum potential theory (MPT) applied to $\mathbf{m} \equiv \rho \mathbf{u}$.

To quantify non-potential contamination, we define the dimensionless leakage field

$$\mathcal{L}(\mathbf{x}) \equiv \frac{|\mathcal{R}(\mathbf{x})|}{\|\nabla \mathbf{u}_{\text{ac}}(\mathbf{x})\|_F + \epsilon_{\text{tol}}}, \quad \epsilon_{\text{tol}} \ll 1, \quad (13)$$

where $\|\nabla \mathbf{u}_{\text{ac}}\|_F$ is the Frobenius norm of the acoustic-velocity Jacobian and ϵ_{tol} prevents division by near-zero gradients. The residual \mathcal{R} is method-specific:

$$\mathcal{R}_{\text{std}} \equiv |(\nabla \times \mathbf{u}_{\text{ac}})_{\text{E}}|, \quad (14)$$

$$\mathcal{R}_{\text{cov}} \equiv |\zeta_{\text{cov}}|. \quad (15)$$

For Doak’s MPT we use the standard momentum split $\mathbf{m} \equiv \rho \mathbf{u} = -\nabla \psi + \mathbf{B}$ with

$$\Delta \psi = -\nabla \cdot \mathbf{m}, \quad \nabla \cdot \mathbf{B} = 0. \quad (16)$$

Because MPT is posed in momentum space, its native non-acoustic remainder is \mathbf{B} . To compare against velocity-based vorticity diagnostics on the same scale, we define a velocity-equivalent potential component using a smooth background density $\rho_0(\mathbf{x})$,

$$\mathbf{u}_{\text{ac}}^{\text{MPT}} \equiv -\frac{1}{\rho_0} \nabla \psi, \quad (17)$$

and report the corresponding vorticity residual

$$\mathcal{R}_{\text{MPT}} \equiv |(\nabla \times \mathbf{u}_{\text{ac}}^{\text{MPT}})_{\text{E}}| = \left| \nabla \left(\frac{1}{\rho_0} \right) \times \nabla \psi \right|. \quad (18)$$

Equation (18) makes explicit that, in inhomogeneous media, a velocity-equivalent MPT field is not generically irrotational even when $\nabla \times \nabla \psi = 0$.

Entropy spot— Thermal nonuniformities (e.g., heat release in reacting flows) create localized entropy spots that strongly refract sound via ∇c_0 without introducing true vortical motion, making them a clean stress test for spurious solenoidal leakage under Euclidean post-processing. Figure 2 visualizes the interaction of a plane acoustic wave with a thermal entropy spot. The spatial variation of $c_0(\mathbf{x})$ causes geodesic refraction of the wavefronts

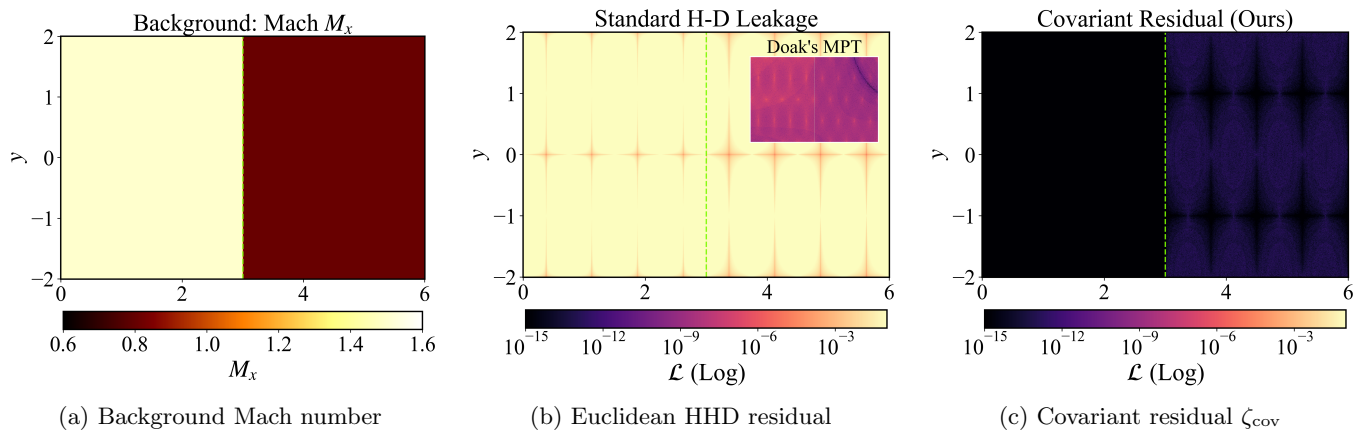


FIG. 4: Separation across a normal shock ($M = 1.5 \rightarrow 0.7$). (a) Background Mach number showing the discontinuity at $x = 3.0$. (b) Euclidean Helmholtz–Hodge post-processing produces a vortex-sheet-like artifact at the shock and contaminates the downstream region. Inset: Doak’s MPT diagnostic. (c) The covariant formulation yields negligible residuals throughout the domain, demonstrating robustness against shock discontinuities.

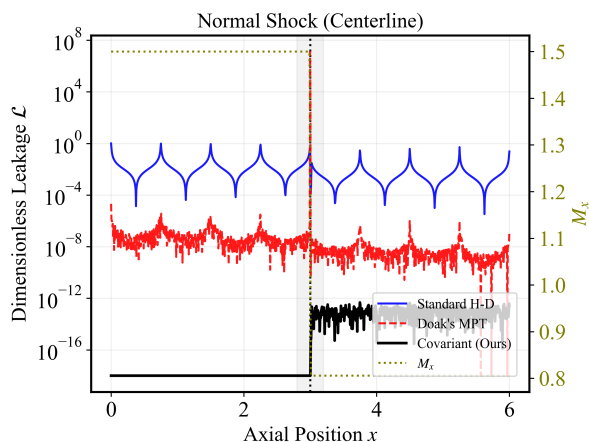


FIG. 5: Shock-wave validation (centerline leakage). Centerline $\mathcal{L}(x, y = 0)$ defined by Eq. (13). Euclidean HHD produces a persistent error plateau downstream of the shock, and Doak’s MPT exhibits spurious oscillatory spikes at the shock location, whereas the covariant residual maintains negligible residuals ($\mathcal{L} \lesssim 10^{-12}$) even at the shock location, eliminating the spurious artifacts observed in other methods.

(Fig. 2a). In a standard Euclidean framework, this geometric bending yields a nonzero apparent curl, which Euclidean HHD misclassifies as solenoidal content. This results in visible contamination in the residual maps and significant leakage in the refracting region (Figs. 2b and 3). Doak’s MPT reduces leakage in the far field but exhibits a broad, pronounced elevation inside the thermal lens where the background density gradient is large, consistent with the $\nabla\rho_0$ term in Eq. (18) (Fig. 3). In contrast, the covariant residual remains at the numerical floor, yielding negligible residuals at the numerical noise

level ($\mathcal{L} \lesssim 10^{-12}$) throughout the domain regardless of the refraction intensity (Figs. 2c and 3).

Normal shock— A normal shock provides a canonical high-gradient test case, effectively representing a singular curvature event in the acoustic metric. Across this discontinuity (Fig. 4a), Euclidean HHD misinterprets the metric jump as a physical vortex sheet, producing a strong localized spike that pollutes the downstream potential field with a persistent error plateau (Figs. 4b and 5). Doak’s MPT, while mathematically consistent for momentum density, inherently incorporates the sharp density gradient into its solenoidal component. When interpreted as an aeroacoustic diagnostic, this manifests as thermodynamic contamination: high-amplitude oscillatory residuals localized at the shock that obscure the true kinematic state (Fig. 5). In contrast, the covariant method yields negligible residuals throughout the domain. By identifying the potential component with the exact part of the metric-dual 1-form, the formulation absorbs the shock discontinuity into the effective geometry. Consequently, combined with the consistent horizon regularization, the metric-aligned splitting maintains separation at the numerical noise floor ($\mathcal{L} \leq 10^{-12}$) even across the singularity, proving that the flow remains irrotational with respect to its own shock-deformed metric (Figs. 4c and 5).

Conclusion— We have shown that the ambiguity in identifying vortical structures in thermodynamically non-uniform media is largely a consequence of applying Euclidean operators to non-Euclidean propagation physics. The present approach generalizes the standard Helmholtz–Hodge splitting to the acoustically privileged metric induced by the analogue-gravity (Gordon) description of sound. In this metric-aligned geometry, the irrotational (potential) component is identified with the

exact part of the metric-dual velocity one-form, ensuring that refraction by ∇c_0 and mean-flow anisotropy are represented as curvature of the effective manifold rather than as spurious solenoidal content. Across both entropy-spot refraction and normal-shock benchmarks, conventional Euclidean and momentum-potential diagnostics exhibit significant leakage, whereas the covariant method maintains separation at the numerical noise floor ($\mathcal{L} \leq 10^{-12}$) throughout the domain. This robustness extends to the metric-degenerate sonic horizon, where entropy gradients physically shift the singularity and consistent regularization ensures a well-posed projection, effectively preventing downstream contamination of the extracted potential field.

While the present work resolves the geometric ambiguity in the velocity field, the complete isolation of non-propagating entropy modes requires a full thermodynamic state vector. A covariant generalization of the Chu–Kovaszny decomposition, built upon this metric framework, will be addressed in a future study to handle multi-variable mode mixing in reacting and high-speed flows. More broadly, this framework is applicable whenever a wave system admits an effective geometric inner product induced by the principal part of the linearized propagation operator. For vector waves with multiple polarizations (*e.g.*, elasticity), the separation becomes tensor-weighted and mode-specific rather than a single-metric gradient/curl splitting. The metric-aware formulation thus provides a practical route to snapshot-based mode isolation in extreme thermo-fluid environments, including high-speed jets, shock–turbulence interaction datasets, and reacting-flow acoustics.

Acknowledgments— The authors are grateful to Professor Ray-Sing Lin for his continuous and enlightening discussions regarding fluid decomposition and aeroacoustics, which provided the foundation for this research.

-
- [1] A. D. Pierce, *Acoustics: an introduction to its physical principles and applications*, 3rd ed. (Springer, 2019).
- [2] M. E. Goldstein, *Aeroacoustics* (McGraw-Hill, 1976).
- [3] D. G. Crighton, A. P. Dowling, J. E. Ffowcs Williams, M. Heckl, and F. G. Leppington, *Modern Methods in Analytical Acoustics: Lecture Notes* (Springer, 1992).
- [4] C. K. W. Tam, *Computational aeroacoustics: A wave number approach*, Cambridge Aerospace Series No. 33 (Cambridge University Press, 2012).
- [5] M. J. Lighthill, On sound generated aerodynamically I. general theory, *Proceedings of the Royal Society of London. Series A. Mathematical and Physical Sciences* **211**, 564 (1952).
- [6] M. J. Lighthill, On sound generated aerodynamically II. turbulence as a source of sound, *Proceedings of the Royal Society of London. Series A. Mathematical and Physical Sciences* **222**, 1 (1954).
- [7] N. Curle, The influence of solid boundaries upon aerodynamic sound, *Proceedings of the Royal Society of London. Series A. Mathematical and Physical Sciences* **231**, 505 (1955).
- [8] J. E. Ffowcs Williams and D. L. Hawkings, Sound generation by turbulence and surfaces in arbitrary motion, *Philosophical Transactions of the Royal Society of London. Series A, Mathematical and Physical Sciences* **264**, 321 (1969).
- [9] S. K. Lele, Computational aeroacoustics: A review, in *35th Aerospace Sciences Meeting and Exhibit* (1997) aIAA Paper 1997-0018.
- [10] T. Colonius and S. K. Lele, Computational aeroacoustics: progress on nonlinear problems of sound generation, *Progress in Aerospace Sciences* **40**, 345 (2004).
- [11] C. K. W. Tam, Supersonic jet noise, *Annual Review of Fluid Mechanics* **27**, 17 (1995).
- [12] J. Boudet, N. Grosjean, and M. C. Jacob, Wake-airfoil interaction as broadband noise source: a large-eddy simulation study, *International Journal of Aeroacoustics* **4**, 93 (2005).
- [13] D. C. Pridmore-Brown, Sound propagation in a fluid flowing through an attenuating duct, *Journal of Fluid Mechanics* **4**, 393 (1958).
- [14] H. Bhatia, G. Norgard, V. Pascucci, and P.-T. Bremer, The Helmholtz-Hodge decomposition—a survey, *IEEE Transactions on Visualization and Computer Graphics* **19**, 1386 (2013), published online 2012, Issue date 2013.
- [15] H. Bhatia, V. Pascucci, and P.-T. Bremer, The natural Helmholtz-Hodge decomposition for open-boundary flow analysis, *IEEE Transactions on Visualization and Computer Graphics* **20**, 1566 (2014).
- [16] S. Schoder, K. Roppert, and M. Kaltenbacher, Post-processing of direct aeroacoustic simulations using Helmholtz decomposition, *AIAA Journal* **58**, 3019 (2020).
- [17] P. Maurerlehner, S. Schoder, J. Tieber, C. Freidhager, H. Steiner, G. Brenn, K.-H. Schäfer, A. Ennemoser, and M. Kaltenbacher, Aeroacoustic formulations for confined flows based on incompressible flow data, *Acta Acustica* **6**, 45 (2022).
- [18] S. Han, H. Li, Y. Luo, Y. Wang, R. Ma, and S. Zhang, A hydro-acoustic mode decomposition method for velocity and pressure field and application to a subsonic turbulent jet, *Physics of Fluids* **35**, 076107 (2023).
- [19] P. E. Doak, Momentum potential theory of energy flux carried by momentum fluctuations, *Journal of Sound and Vibration* **131**, 67 (1989).
- [20] P. E. Doak, Fluctuating total enthalpy as the basic generalized acoustic field, *Theoretical and Computational Fluid Dynamics* **10**, 115 (1998).
- [21] P. Jordan, G. Daviller, and P. Comte, Doak’s momentum potential theory of energy flux used to study a solenoidal wavepacket, *Journal of Sound and Vibration* **332**, 3924 (2013).
- [22] A. Powell, Theory of vortex sound, *The Journal of the Acoustical Society of America* **36**, 177 (1964).
- [23] M. S. Howe, Contributions to the theory of aerodynamic sound, with application to excess jet noise and the theory of the flute, *Journal of Fluid Mechanics* **71**, 625 (1975).
- [24] W. Möhring, On vortex sound at low Mach number, *Journal of Fluid Mechanics* **85**, 685 (1978).
- [25] M. S. Howe, *Acoustics of fluid-structure interactions*, Cambridge Monographs on Mechanics (Cambridge University Press, 1998).

- [26] T. Suzuki and T. Colonius, Instability waves in a subsonic round jet detected using a near-field phased microphone array, *Journal of Fluid Mechanics* **565**, 197 (2006).
- [27] P. Jordan and T. Colonius, Wave packets and turbulent jet noise, *Annual Review of Fluid Mechanics* **45**, 173 (2013).
- [28] A. Towne, O. T. Schmidt, and T. Colonius, Spectral proper orthogonal decomposition and its relationship to dynamic mode decomposition and resolvent analysis, *Journal of Fluid Mechanics* **847**, 821 (2018).
- [29] O. T. Schmidt, A. Towne, G. Rigas, T. Colonius, and G. A. Brès, Spectral analysis of jet turbulence, *Journal of Fluid Mechanics* **855**, 953 (2018).
- [30] R. Ewert and W. Schröder, Acoustic perturbation equations based on flow decomposition via source filtering, *Journal of Computational Physics* **188**, 365 (2003).
- [31] R. Ewert and J. Kreuzinger, Hydrodynamic/acoustic splitting approach with flow-acoustic feedback for universal subsonic noise computation, *Journal of Computational Physics* **444**, 110548 (2021).
- [32] D. Blokhintzev, The propagation of sound in an inhomogeneous and moving medium I, *The Journal of the Acoustical Society of America* **18**, 322 (1946).
- [33] D. Blokhintzev, The propagation of sound in an inhomogeneous and moving medium II, *The Journal of the Acoustical Society of America* **18**, 329 (1946).
- [34] V. E. Ostashev and D. K. Wilson, *Acoustics in moving inhomogeneous media*, 2nd ed. (CRC Press, 2015).
- [35] H. S. Ribner, *Convection of a Pattern of Vorticity Through a Shock Wave*, Tech. Rep. NACA TR 1164 (National Advisory Committee for Aeronautics, Washington, D.C., 1954).
- [36] J. Ryu and D. Livescu, Direct numerical simulations of isotropic turbulence interacting with a shock wave, in *29th International Symposium on Shock Waves 2*, edited by R. Bonazza and D. Ranjan (Springer International Publishing, Cham, 2015) pp. 1423–1428.
- [37] J. Larsson, I. Bermejo-Moreno, and S. K. Lele, Reynolds- and Mach-number effects in canonical shock–turbulence interaction, *Journal of Fluid Mechanics* **717**, 293 (2013).
- [38] J. M. Bardeen, Gauge-invariant cosmological perturbations, *Physical Review D* **22**, 1882 (1980).
- [39] J. B. Pendry, D. Schurig, and D. R. Smith, Controlling electromagnetic fields, *Science* **312**, 1780 (2006).
- [40] J. Dellinger and J. Etgen, Wave-field separation in two-dimensional anisotropic media, *Geophysics* **55**, 914 (1990).
- [41] W. Gordon, Zur Lichtfortpflanzung nach der Relativitätstheorie, *Annalen der Physik* **377**, 421 (1923).
- [42] W. G. Unruh, Experimental black-hole evaporation?, *Physical Review Letters* **46**, 1351 (1981).
- [43] M. Visser, Acoustic black holes: horizons, ergospheres and Hawking radiation, *Classical and Quantum Gravity* **15**, 1767 (1998).
- [44] C. Barceló, S. Liberati, and M. Visser, Analogue gravity, *Living Reviews in Relativity* **14**, 3 (2011).
- [45] G. E. Volovik, *The Universe in a Helium Droplet* (Oxford University Press, 2009).
- [46] M. Stone, Acoustic energy and momentum in a moving medium, *Physical Review E* **62**, 1341 (2000).

End Matter

Appendix A: Theoretical Generalization: Monolithic Variational Solution—

1. *Variational Formulation.* For general applications beyond the canonical benchmarks presented in the main text, let (\mathcal{M}, γ) be the Riemannian manifold induced by the acoustic metric. We seek the decomposition $\mathbf{u}^b = d\phi + \delta\Psi + \mathbf{h}$ (where \mathbf{h} is harmonic) by minimizing the residual kinetic energy functional E with respect to the scalar potential ϕ (0-form) and the vector potential Ψ (2-form in 3D). Note that in this section, δ denotes the codifferential operator (adjoint of d), to be distinguished from the variational perturbation denoted by $\delta(\cdot)$.

$$E[\phi, \Psi] = \frac{1}{2} \int_{\Omega} \left\| \mathbf{u}^b - d\phi - \delta\Psi \right\|_{\gamma}^2 dV_{\gamma}. \quad (19)$$

Taking the first variation with respect to ϕ and Ψ independently yields the stationarity conditions:

$$\delta_{\phi} E = -\langle \mathbf{u}^b - d\phi - \delta\Psi, d(\delta\phi) \rangle_{\gamma} = 0, \quad (20a)$$

$$\delta_{\Psi} E = -\langle \mathbf{u}^b - d\phi - \delta\Psi, \delta(\delta\Psi) \rangle_{\gamma} = 0. \quad (20b)$$

2. *Derivation of the Coupled System.* Using the Green’s formula for differential forms, $\langle \alpha, d\beta \rangle_{\Omega} = \langle \delta\alpha, \beta \rangle_{\Omega} + \oint_{\partial\Omega} \alpha \wedge \star\beta$, we integrate (20a) and (20b) by parts. Noting that the operators are nilpotent ($\delta^2 = 0$

and $d^2 = 0$), the interior terms decouple into the standard Poisson and vector-potential equations:

$$\begin{cases} \delta d\phi = \delta\mathbf{u}^b & \text{(Scalar Laplacian),} \\ d\delta\Psi = d\mathbf{u}^b & \text{(Vector Laplacian).} \end{cases} \quad (21)$$

However, the boundary terms generically couple the potentials. The condition $\delta E = 0$ for arbitrary perturbations $(\delta\phi, \delta\Psi)$ on the boundary implies natural boundary conditions:

$$\oint_{\partial\Omega} (\mathbf{u}^b - d\phi - \delta\Psi) \wedge \star\delta\Psi + \oint_{\partial\Omega} \star(\mathbf{u}^b - d\phi - \delta\Psi) \wedge \delta\phi = 0. \quad (22)$$

This explicitly shows that the flux \mathbf{u}^b at the boundary is optimally partitioned between the exact ($d\phi$) and coexact ($\delta\Psi$) components to minimize the global energy norm.

3. *Monolithic Linear Structure.* Discretizing the variational forms leads to a symmetric block linear system of the form $\mathbf{A}\mathbf{x} = \mathbf{b}$:

$$\begin{bmatrix} \mathbf{L}_{\phi\phi} & \mathbf{C}_{\phi\Psi} \\ \mathbf{C}_{\Psi\phi} & \mathbf{L}_{\Psi\Psi} \end{bmatrix} \begin{pmatrix} \phi \\ \Psi \end{pmatrix} = \begin{pmatrix} \mathbf{D}^T \mathbf{M} \mathbf{u} \\ \mathbf{C}^T \mathbf{M} \mathbf{u} \end{pmatrix}, \quad (23)$$

where $\mathbf{L}_{\phi\phi}$ and $\mathbf{L}_{\Psi\Psi}$ represent the metric-weighted Laplacian operators (stiffness matrices), and $\mathbf{C}_{\phi\Psi}$ represents

the boundary coupling matrix. On the right-hand side, \mathbf{D}^T and \mathbf{C}^T denote the discrete divergence and curl (codifferential) operators acting on the velocity vector \mathbf{u} . Crucially, the matrix \mathbf{A} depends only on the metric γ_{ij} and the mesh topology. Therefore, the potentials ϕ and Ψ are determined simultaneously by a single inversion (or Krylov subspace solve) of \mathbf{A} . This confirms that the covariant Natural HHD is an iteration-free, linear projection method.

Appendix B: Numerical Implementation— All benchmarks are evaluated on a uniform Cartesian grid. Discrete spatial derivatives are formed as Kronecker products of one-dimensional second-order central-difference matrices in the interior, with one-sided stencils on the outermost points. To ensure discrete consistency between the divergence and gradient, the covariant Laplace–Beltrami operator is assembled explicitly in conservative form:

$$(\Delta_g \phi) \approx \frac{1}{\sqrt{\gamma}} \left[D_x (\sqrt{\gamma} \gamma^{xx} D_x \phi + \sqrt{\gamma} \gamma^{xy} D_y \phi) + D_y (\sqrt{\gamma} \gamma^{yx} D_x \phi + \sqrt{\gamma} \gamma^{yy} D_y \phi) \right], \quad (24)$$

which guarantees that the numerical residual vanishes exactly for pure potential fields. The natural Neumann condition $(\nabla_\gamma \phi) \cdot \mathbf{n} = \mathbf{u}' \cdot \mathbf{n}$ is imposed; in the present benchmarks, disturbances decay to negligible amplitude near the outer boundary, rendering the condition effectively homogeneous. To ensure a unique solution, the null space is removed by fixing the potential at a single reference grid point (gauge fixing). In the context of the generalized variational formulation (Appendix A), we note that the vector potential Ψ admits a gauge freedom that renders the system singular; invertibility is theoretically restored by applying a compatible gauge condition (*e.g.*, fixing specific nodal values or enforcing a discrete Coulomb gauge). The resulting sparse symmetric linear systems are solved using the Conjugate Gradient (CG) method with a relative tolerance of 10^{-10} . Near sonic horizons where the metric becomes singular, the determinant factor is regularized by enforcing $\beta_{\text{safe}} =$

$\max(c_0^2 - |\mathbf{U}_0|^2, \epsilon_{\text{reg}}^2)$ with $\epsilon_{\text{reg}}^2 = 10^{-16} \max_{\mathbf{x} \in \Omega}(c_0^2)$.

Appendix C: Entropy Spot Benchmark— The computational domain is $(x, y) \in [0, 4] \times [-2, 2]$ with a grid resolution of $N_x \times N_y = 800 \times 800$. The background state consists of a Gaussian thermal lens superimposed on a shear flow:

$$c_0(x, y) = 340 + 70 \exp[-4((x-2)^2 + y^2)], \quad (25)$$

$$U_0(y) = 150 \tanh(2y), \quad V_0 = 0, \quad (26)$$

(units in m/s). The isobaric density profile follows $\rho_0(x, y) \propto c_0^{-2}$. The prescribed acoustic potential is a localized wave packet modulated by a Gaussian envelope:

$$\phi(x, y) = \sin\left(\frac{3\pi x}{4}\right) \cos\left(\frac{3\pi y}{4}\right) \exp[-0.5((x-2)^2 + y^2)]. \quad (27)$$

This configuration probes leakage induced by strong, spatially varying acoustic geometry (via c_0) and mean shear (U_0).

Appendix D: Normal Shock Benchmark— The domain is $(x, y) \in [0, 6] \times [-2, 2]$ with a resolution of $N_x \times N_y = 1200 \times 800$. A normal shock is located at $x_s = 3.0$ with an upstream Mach number $M_{\text{up}} = 1.5$. The downstream state is determined by the Rankine–Hugoniot relations for the specific heat ratio $\Gamma = 1.4$. To mimic a resolved shock structure, the background velocity profile is smoothed using a Gaussian filter, approximating a viscous shock thickness:

$$U_0(x) \approx \frac{U_{\text{up}} + U_{\text{dn}}}{2} - \frac{U_{\text{up}} - U_{\text{dn}}}{2} \tanh\left(\frac{x - x_s}{\delta}\right). \quad (28)$$

The acoustic perturbation corresponds to a plane-wave packet passing through the shock:

$$\phi(x, y) = \sin\left(\frac{4\pi x}{3}\right) \cos\left(\frac{\pi y}{2}\right). \quad (29)$$

This benchmark tests robustness in the presence of sharp gradients and near-degenerate metric coefficients within the shock layer.